3D-QSAR studies of checkpoint kinase 1 inhibitors based on molecular docking and CoMFA

Rong Wei Wang[a]; Lu Zhou[a]; Zhili Zuo[bc]; Xiang Ma[a]; Min Yang[a]

[a] College of Chemical Engineering, Sichuan University, Sichuan, Chengdu, P.R. China [b] Centre for Biomedical and Life Sciences, Singapore Polytechnic, Singapore, Singapore [c] School of Biomedical Sciences, Curtin University of Technology, Perth, WA, Australia

PLEASE SCROLL DOWN FOR ARTICLE

Taylor & Francis
Taylor & Francis Group

3D-QSAR studies of checkpoint kinase 1 inhibitors based on molecular docking and CoMFA

Rong Wei Wang[a], Lu Zhou[a]*, Zhili Zuo[bc1], Xiang Ma[a] and Min Yang[a]

[a]College of Chemical Engineering, Sichuan University, Sichuan, Chengdu 610065, P.R. China; [b]Centre for Biomedical and Life Sciences, Singapore Polytechnic, Singapore 139651, Singapore; [c]School of Biomedical Sciences, Curtin University of Technology, Perth, WA 6485, Australia

Three-dimensional quantitative structure–activity relationship (3D-QSAR) studies were performed on a series of substituted 1,4-dihydroindeno[1,2-c]pyrazoles inhibitors, using molecular docking and comparative molecular field analysis (CoMFA). The docking results from GOLD 3.0.1 provide a reliable conformational alignment scheme for the 3D-QSAR model. Based on the docking conformations and alignments, highly predictive CoMFA model was built with cross-validated q^2 value of 0.534 and non-cross-validated partial least-squares analysis with the optimum components of six showed a conventional r^2 value of 0.911. The predictive ability of this model was validated by the testing set with a conventional r^2 value of 0.812. Based on the docking and CoMFA, we have identified some key features of the 1,4-dihydroindeno[1,2-c]pyrazoles derivatives that are responsible for checkpoint kinase 1 inhibitory activity. The analyses may be used to design more potent 1,4-dihydroindeno[1,2-c]pyrazoles derivatives and predict their activity prior to synthesis.

Keywords: CoMFA; 3D-QSAR; checkpoint kinase 1 (CHK1); molecular docking; substituted 1,4-dihydroindeno[1,2-c]pyrazoles

1. Introduction

DNA-damaging anticancer agent is the most important cancer treatment and has significantly increased the survival of cancer patients when used in combination with drugs with different mechanisms [1]. However, the clinical use of DNA-damaging anticancer agent is limited by its severe toxicity and resistance from tumour cells. So, it is important to develop highly efficient and less toxic drugs for cancer, which may either sensitise tumour tissues or protect normal tissues from DNA damage [2].

With DNA damage, cells are arrested at G1, S or G2 phase to initiate the DNA repair process [3–5]. Most tumour cells distinguish themselves from normal cells by lacking the G1 checkpoint due to the loss of p53, and therefore they are selectively arrested at the S or G2 checkpoint after DNA damage. If the S and G2 checkpoints are abrogated, G1-deficient cancer cells will die. In contrast, normal cells are still arrested in the G1 phase and are less affected by S and G2 checkpoint abrogation, suggesting that a favourable therapeutic window should be achieved for G2 and/or S abrogations [6].

Checkpoint kinase 1 (CHK1) is a serine/threonine protein kinase and key mediator in the DNA damage-induced checkpoint network, and it is activated via activation of the upstream ATM/ATR pathway [7–10]. Activation of CHK1 results in phosphorylation of Cdc25A at Ser123, Cdc25C at Ser216 and several other serine residues. The downstream event is the inhibition of cyclin E/Cdk2 or cyclin B/Cdc2 kinase, which finally results in cell cycle arrest at S or G2 phase [11]. The inhibitors of CHK1 abrogate the S and G2 checkpoints; thereby they preferentially sensitise tumour cells, especially p53-null cells. Consequently, CHK1 has emerged as an attractive chemosensitisation target, and the inhibitors of CHK1 may significantly improve the efficacy and selectivity of DNA-damaging agents [6].

In recent years, a number of CHK1 inhibitors have been reported, including indolocarbazoles [12], isogranulatimides [13], debromohymenialdisines [14], aminopyrimidines [15], pyrrolopyridines [16], benzimidazole-quinolinones [17], indazoles [18], diarylureas [6] and macrocyclic ureas [19]. Based on a hit identified from high-throughput screening, Yunsong Tong et al. found that *N*-((3-(4-fluorophenyl)-2,4-dihydroindeno[1,2-c]pyrazol-6-yl)methyl)-1-methylpiperidin-4-amine is a potent inhibitor of CHK1 with IC_{50} of 510 nM [19]. Moreover, they synthesised a series of 1,4-dihydroindeno[1,2-c]pyrazoles derivatives as potent and selective CHK1 inhibitors [2,11,19,20]. The binding mode of CHK2759M41 has been determined by X-ray crystallography, which provided not only insights into the interaction mechanisms of CHK1 with the inhibitors, but also valuable clues for designing new inhibitors. In this paper, with the molecular docking and comparative molecular field analysis (CoMFA), it is possible to get

*Corresponding author. Email: zhoulu@scu.edu.cn

new insights into the relationship between the structural information of a series of substituted 1,4-dihydroindeno[1,2-c]pyrazoles inhibitors and the inhibitory potency, and structural features in CHK1 were identified, which can be used to design new inhibitors (Table 1).

2.   Computational details

2.1   *Biological activity and molecular structures*

A panel of 151 structurally and pharmacologically diverse compounds was selected for the three-dimensional quantitative structure–activity relationship (3D-QSAR) analysis, and all of them are from four publications reported by one laboratory [2,11,19,20]. Because of the same experimental procedures applied for affinity determination in each publication, the biological data (represented as IC_{50} values) were considered comparable and thus merged into our study. Inhibitors without exact IC_{50} value (indicated with $> 10,000\,nM$) were omitted. The compounds were divided into a training set and a testing set as shown in Tables 1 and 2. The training set consists of 121 compounds and the testing set comprised 30 compounds, which were selected randomly. The IC_{50} values were converted to pIC_{50} ($-\log IC_{50}$) values which were used as dependent variables in the QSAR analyses. The pIC_{50} values of the compounds cover an interval of more than three log units [21].

The 3D structures of these compounds were built using SYBYL 8.0 (Tripos Associates, Inc., St Louis, MO, USA). Partial atomic charges were calculated by the Gasteiger–Hückel method and energy minimisations were performed using the Tripos force field with a distance-dependent dielectric and the Powell conjugate gradient algorithm with a convergence criterion of 0.005 kcal/mol/Å.

2.2   *Docking studies*

To locate the appropriate binding orientations and conformations of these 1,4-dihydroindeno[1,2-c]pyrazoles inhibitors interacting with CHK1, a powerful computational searching method is needed. The advanced molecular docking program GOLD (version 3.0.1), with a powerful genetic algorithm (GA) method for conformational search and docking programs [22], was employed to generate an ensemble of docked conformations. Atomic coordinates for the CHK1 complex with 76A (compound CHK2759M41) were extracted from the Protein Databank with a resolution of 2.5 Å (PDB ID: 2E9N). The original ligand was extracted from the crystal structure. The genetic operators were 100 for the population size, 1.1 for the selection, 5 for the number of subpopulations, 100,000 for the maximum number of genetic applications and 2 for the size of the niche used to increase population diversity. The weights were chosen so

that crossover mutations were applied with equal probability (95/95 for the values) and migration was applied 5% of the time [23].

2.3   *Choice of docking fitness functions*

The ChemScore function described by Eldridge and others [24,25] and encoded in GOLD was applied to predict the binding positions between the CHK1 and 151 inhibitors. ChemScore estimates the total free energy change that occurs on ligand binding as:

$$\Delta G_{binding} = \Delta G_0 + \Delta G_{hbond} + \Delta G_{metal} + \Delta G_{lipo}$$
$$+ \Delta G_{rot}. \tag{1}$$

After adding in a clash penalty and internal torsion terms, the final ChemScore value is then obtained, in which the covalent and constraint scores may also be included. P terms represent the various types of physical contributions to binding.
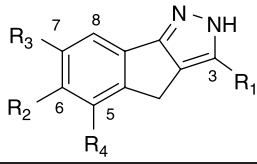
$$Chemscore = \Delta G_{binding} + P_{clash} + c_{internal}P_{internal}$$
$$+ (c_{covalent}P_{covalent} + P_{constraint}). \tag{2}$$

The fitness score is taken as the negative of the sum of the component energy terms, so that larger fitness scores are better [26]. However, there is no statistically significant relationship between the GOLD ChemScore and biological activity for these inhibitors. Since the GOLD fitness function was designed to discriminate different binding modes of the same molecule, maybe extra terms such as entropic loss are required to compare different molecules. Some others' studies also showed that case [27,28]. On the other hand, the ligand–receptor interaction is mediated by other factors such as the flexibility and conformational changes of the receptor during binding with the ligand, which is one of the major difficulties in predicting protein–ligand complexes [29,30]. However, in the version of GOLD used here, only dihedrals of protein OH and NH_3^+ groups are optimised and the protein backbone is not flexible [26]. These features may also explain no statistically significant relationship between the GOLD ChemScore and biological activity.

2.4   *Structural alignment*

Identification of the molecular alignment of compounds is one of the most important steps in 3D-QSAR analysis. In this study, 10 conformations were obtained using GOLD for each ligand. The conformations with the highest ChemScore for each ligand from the training set were aligned together inside the binding

Table 1. Structures and inhibitory activity of 1,4-dihydroindeno[1,2-c]pyrazoles derivatives.
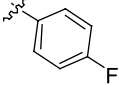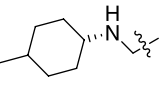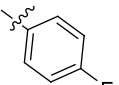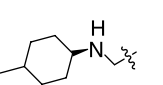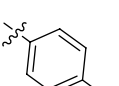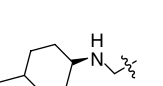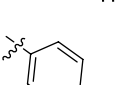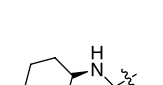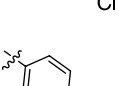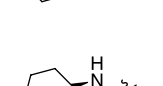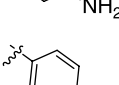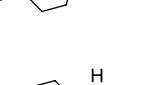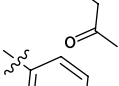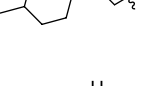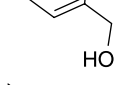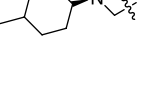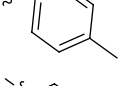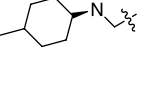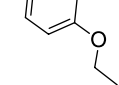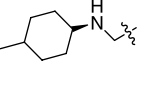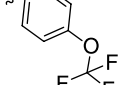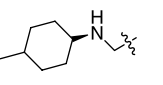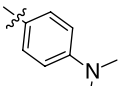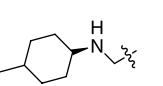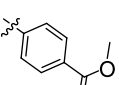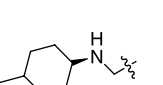

Compounds	R_1	R_2	R_3	R_4	IC_{50} (nM)	$p\,IC_{50}$
CHK2759M7	4-F-phenyl	4-methylcyclohexyl-NH-	H	H	459	6.34
CHK2759M8	4-F-phenyl	4-methylcyclohexyl-NH-	H	H	814	6.09
CHK2759M9	phenyl (H)	4-methylcyclohexyl-NH-	H	H	1473	5.83
CHK2759M10	4-Cl-phenyl	4-methylcyclohexyl-NH-	H	H	481	6.32
CHK2759M11	4-NH$_2$-phenyl	4-methylcyclohexyl-NH-	H	H	1042	5.98
CHK2759M12	4-(CH$_2$COCH$_3$)-phenyl	4-methylcyclohexyl-NH-	H	H	497	6.3
CHK2759M13	4-(CH$_2$OH)-phenyl	4-methylcyclohexyl-NH-	H	H	790	6.1
CHK2759M14	4-CH$_3$-phenyl	4-methylcyclohexyl-NH-	H	H	966	6.02
CHK2759M15	4-OEt-phenyl	4-methylcyclohexyl-NH-	H	H	1600	5.8
CHK2759M16	4-OCF$_3$-phenyl	4-methylcyclohexyl-NH-	H	H	2044	5.69
CHK2759M17	4-N(CH$_3$)$_2$-phenyl	4-methylcyclohexyl-NH-	H	H	5260	5.28
CHK2759M18	4-(COOCH$_3$)-phenyl	4-methylcyclohexyl-NH-	H	H	602	6.22
CHK2759M19	4-OH-phenyl	4-methylcyclohexyl-NH-	H	H	124	6.91

Table 1 – continued
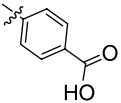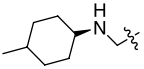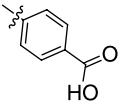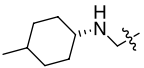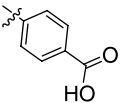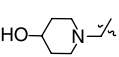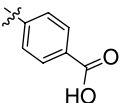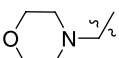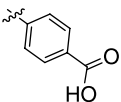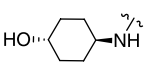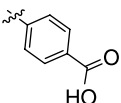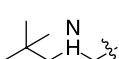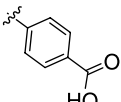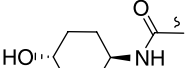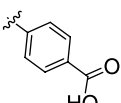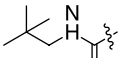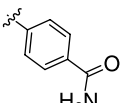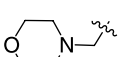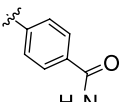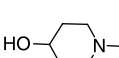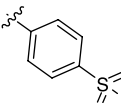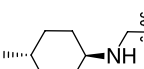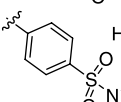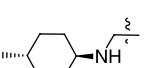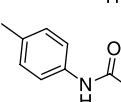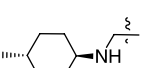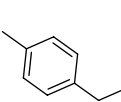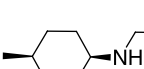
Compounds	R₁	R₂	R₃	R₄	IC$_{50}$ (nM)	pIC$_{50}$
CHK2759M20			H	H	22	7.66
CHK2759M21			H	H	20	7.70
CHK2759M22			H	H	15	7.82
CHK2759M23			H	H	7.9	8.10
CHK2759M24			H	H	6.0	8.22
CHK2759M25			H	H	15	7.82
CHK2759M26			H	H	12	7.92
CHK2759M27			H	H	12	7.92
CHK2759M28			H	H	69	7.16
CHK2759M29			H	H	29	7.54
CHK2759M30			H	H	535	6.27
CHK2759M31			H	H	8742	5.06
CHK2759M32			H	H	4825	5.32
CHK2759M35			H	H	1880	5.73

Table 1 – *continued*
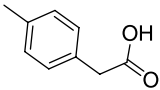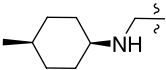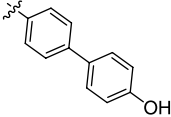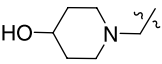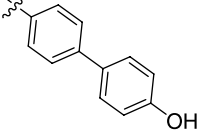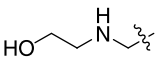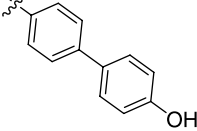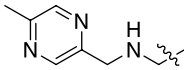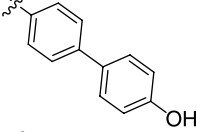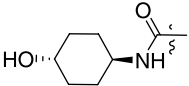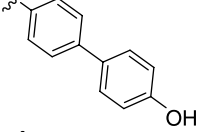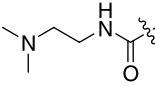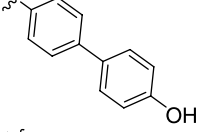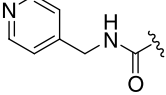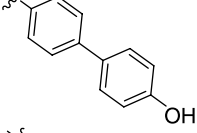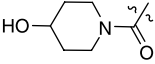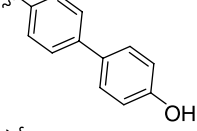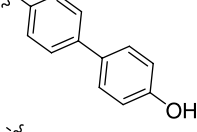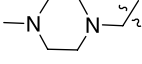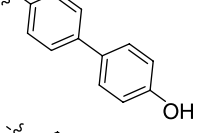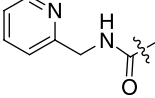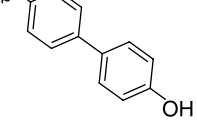
Compounds	R₁	R₂	R₃	R₄	IC₅₀ (nM)	pIC₅₀
CHK2759M36			H	H	6472	5.19
CHK2759M37			H	H	2.0	8.70
CHK2759M38			H	H	6.6	8.18
CHK2759M40			H	H	7.4	8.13
CHK2759M41			H	H	6.2	8.21
CHK2759M42			H	H	4.0	8.40
CHK2759M43			H	H	13	7.89
CHK2759M44			H	H	3.6	8.44
CHK3618M5		H	H	H	1373	5.86
CHK3618M6			H	H	24	7.62
CHK3618M7			H	H	9.3	8.03
CHK3618M8		OH	H	H	4.4	8.36

Table 1 – *continued*
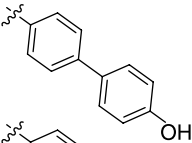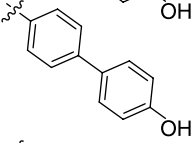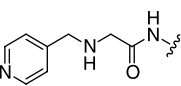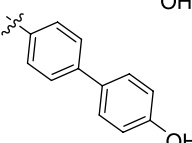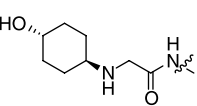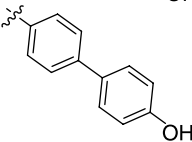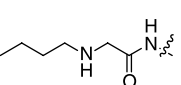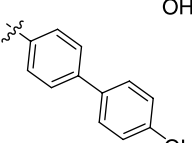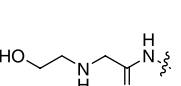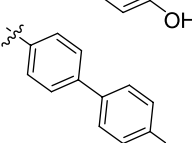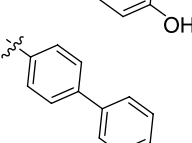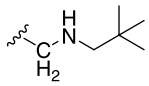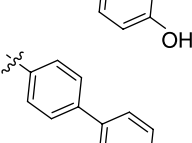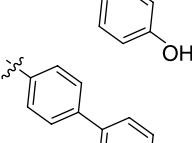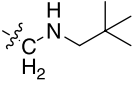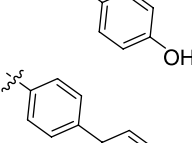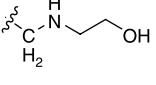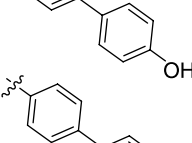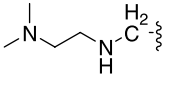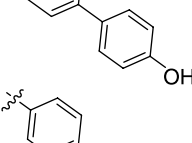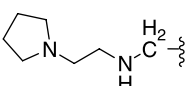
Compounds	R₁	R₂	R₃	R₄	IC₅₀ (nM)	pIC₅₀
CHK3618M9		CH_2OH	H	H	7.7	8.11
CHK3618M10			H	H	6.4	8.19
CHK3618M11			H	H	1.2	8.92
CHK3618M12			H	H	2.1	8.68
CHK3618M13			H	H	0.74	9.13
CHK3618M15		H	H	CH_2OH	7.8	8.11
CHK3618M16		H	H		209	6.68
CHK3618M19		H	CH_2OH	H	4.4	8.36
CHK3618M20		H		H	34	7.47
CHK3618M21		H		H	12	7.92
CHK3618M22		H		H	5.2	7.82
CHK3618M23		H		H	7.1	8.15

Table 1 – *continued*
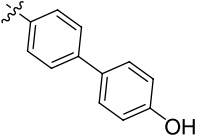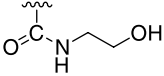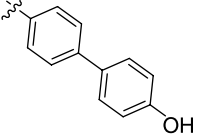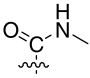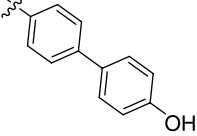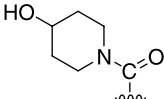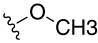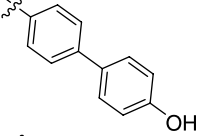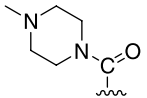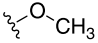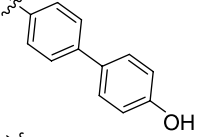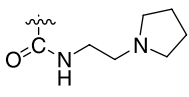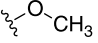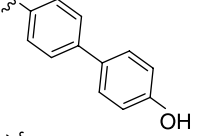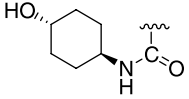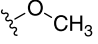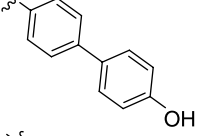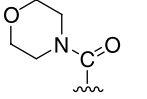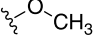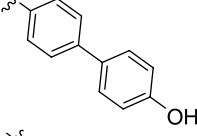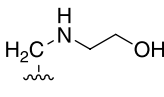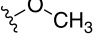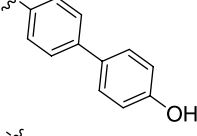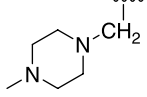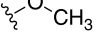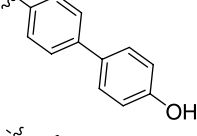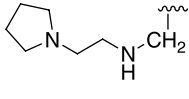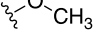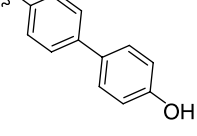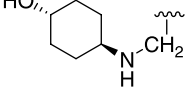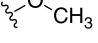
Compounds	R$_1$	R$_2$	R$_3$	R$_4$	IC$_{50}$ (nM)	pIC$_{50}$
CHK3618M24	biphenyl-OH	H	C(=O)NHCH$_2$CH$_2$OH	H	5.0	8.300
CHK3618M25	biphenyl-OH	H	C(=O)NHCH$_3$	H	2.3	8.64
CHK3618M33	biphenyl-OH	4-hydroxypiperidin-1-yl-C(=O)	O-CH3	H	0.24	9.62
CHK3618M34	biphenyl-OH	4-methylpiperazin-1-yl-C(=O)	O-CH3	H	2.3	8.64
CHK3618M35	biphenyl-OH	C(=O)NHCH$_2$CH$_2$-pyrrolidin-1-yl	O-CH3	H	0.83	9.08
CHK3618M36	biphenyl-OH	trans-4-hydroxycyclohexyl-NH-C(=O)	O-CH3	H	0.24	9.62
CHK3618M37	biphenyl-OH	morpholin-4-yl-C(=O)	O-CH3	H	0.55	9.26
CHK3618M38	biphenyl-OH	H$_2$C-NH-CH$_2$CH$_2$OH	O-CH3	H	0.43	9.37
CHK3618M39	biphenyl-OH	4-methylpiperazin-1-yl-CH$_2$	O-CH3	H	0.51	9.29
CHK3618M40	biphenyl-OH	pyrrolidin-1-yl-CH$_2$CH$_2$-NH-CH$_2$	O-CH3	H	0.21	9.68
CHK3618M41	biphenyl-OH	trans-4-hydroxycyclohexyl-NH-CH$_2$	O-CH3	H	0.56	9.25

Table 1 – *continued*
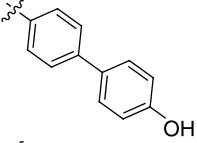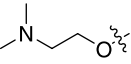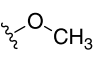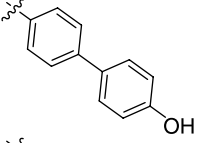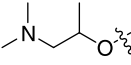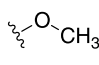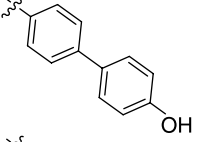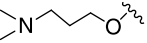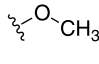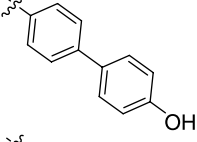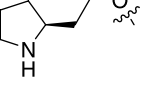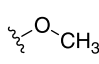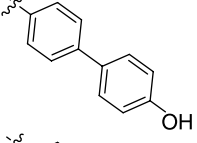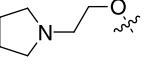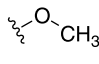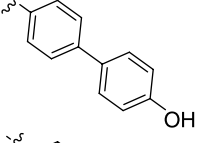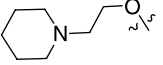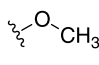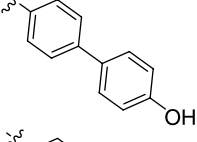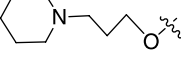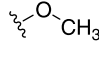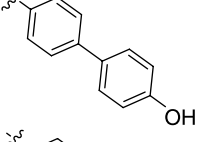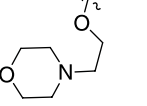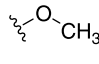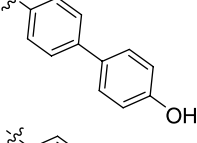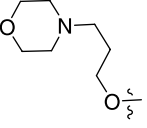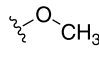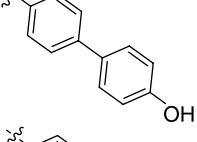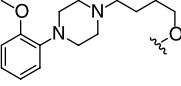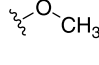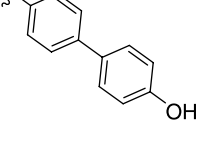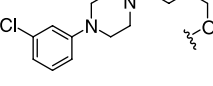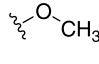
Compounds	R$_1$	R$_2$	R$_3$	R$_4$	IC$_{50}$ (nM)	p IC$_{50}$
CHK4308M5				H	2	8.70
CHK4308M6				H	2	8.70
CHK4308M7				H	0.7	9.15
CHK4308M8				H	2	8.70
CHK4308M9				H	0.8	9.10
CHK4308M10				H	1	9.00
CHK4308M11				H	4	8.40
CHK4308M12				H	2	8.70
CHK4308M13				H	6	8.22
CHK4308M14				H	25	7.60
CHK4308M15				H	8	8.10

Table 1 – *continued*
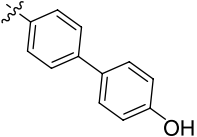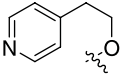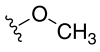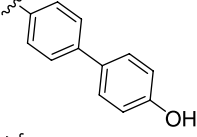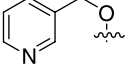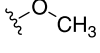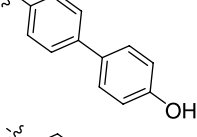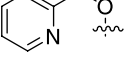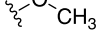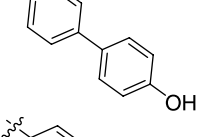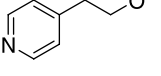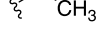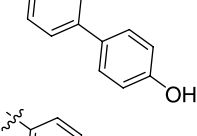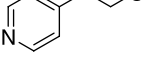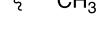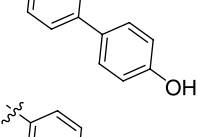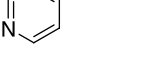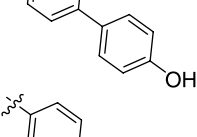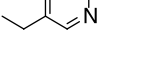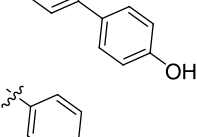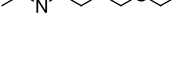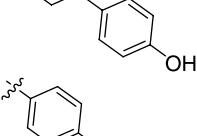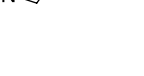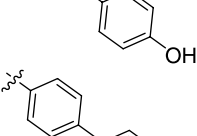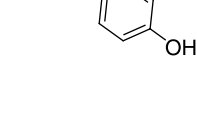
Compounds	R_1	R_2	R_3	R_4	IC_{50} (nM)	$p\,IC_{50}$
CHK4308M16				H	8	8.10
CHK4308M17				H	18	7.74
CHK4308M18				H	20	7.70
CHK4308M19				H	5	8.30
CHK4308M20				H	13	7.89
CHK4308M21				H	30	7.52
CHK4308M22				H	23	7.64
CHK4308M23				H	62	7.21
CHK4308M24				H	5	8.30
CHK4308M26				H	0.1	10.00
CHK4308M27				H	0.1	10.00

Table 1 – *continued*
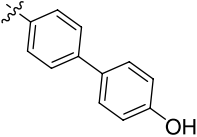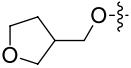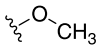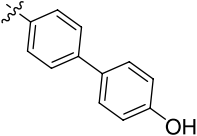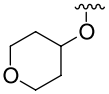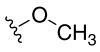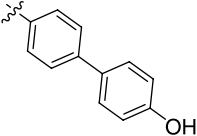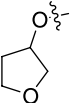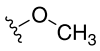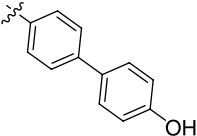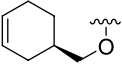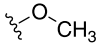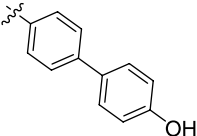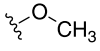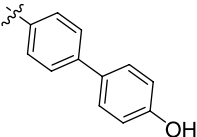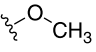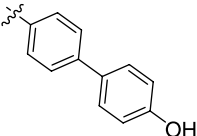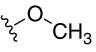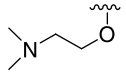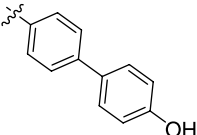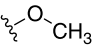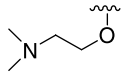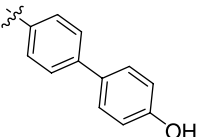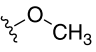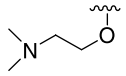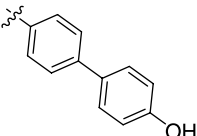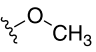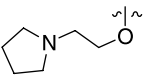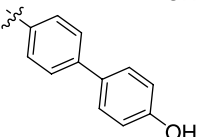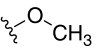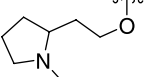
Compounds	R_1	R_2	R_3	R_4	IC_{50} (nM)	pIC_{50}
CHK4308M28			OCH₃	H	0.8	9.10
CHK4308M29			OCH₃	H	0.2	9.70
CHK4308M30			OCH₃	H	0.4	9.40
CHK4308M31			OCH₃	H	0.7	9.15
CHK4308M32		OH	OCH₃	H	1	9.00
CHK4308M33		OCH₃	OH	H	5	8.30
CHK4308M34		OCH₃		H	0.8	9.10
CHK4308M35		OCH₃		H	2	8.70
CHK4308M36		OCH₃		H	0.6	9.22
CHK4308M37		OCH₃		H	2	8.70
CHK4308M38		OCH₃		H	0.8	9.10
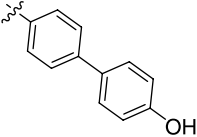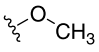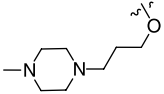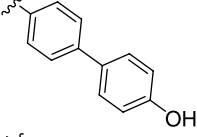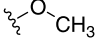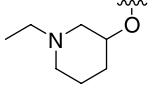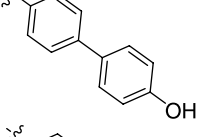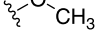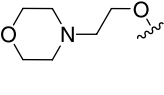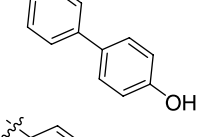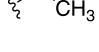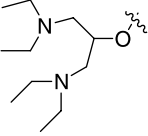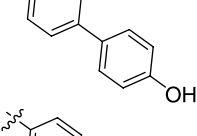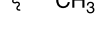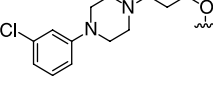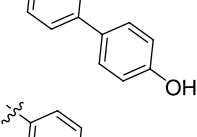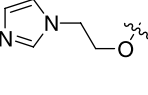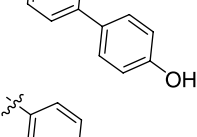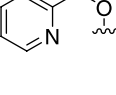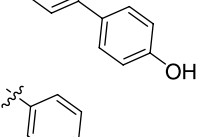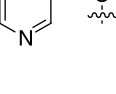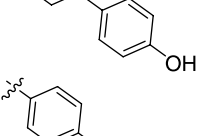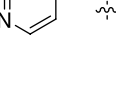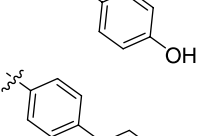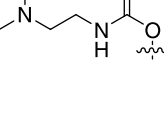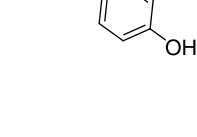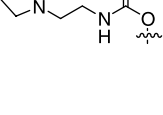
Table 1 – *continued*

Compounds	R$_1$	R$_2$	R$_3$	R$_4$	IC$_{50}$ (nM)	p IC$_{50}$
CHK4308M39	biphenyl-OH	O-CH$_3$	methylpiperazine-propyl-O	H	0.2	9.70
CHK4308M40	biphenyl-OH	O-CH$_3$	ethylpiperidine-O	H	0.6	9.22
CHK4308M41	biphenyl-OH	O-CH$_3$	morpholine-ethyl-O	H	5	8.30
CHK4308M42	biphenyl-OH	O-CH$_3$	bis(diethylamino)-O	H	2	8.70
CHK4308M43	biphenyl-OH	O-CH$_3$	Cl-phenyl-piperazine-propyl-O	H	10	8.00
CHK4308M44	biphenyl-OH	O-CH$_3$	imidazole-ethyl-O	H	3	8.52
CHK4308M45	biphenyl-OH	O-CH$_3$	pyridin-2-yl-methyl-O	H	24	7.62
CHK4308M46	biphenyl-OH	O-CH$_3$	pyridin-3-yl-methyl-O	H	23	7.64
CHK4308M47	biphenyl-OH	O-CH$_3$	pyridin-4-yl-methyl-O	H	36	7.44
CHK4308M48	biphenyl-OH	O-CH$_3$	dimethylamino-ethyl-carbamate-O	H	40	7.40
CHK4308M49	biphenyl-OH	O-CH$_3$	pyrrolidine-ethyl-carbamate-O	H	21	7.68

Table 1 – *continued*
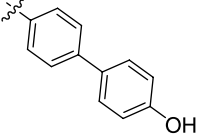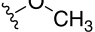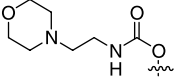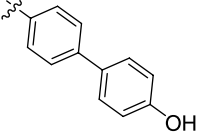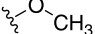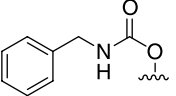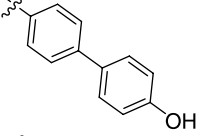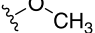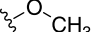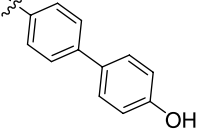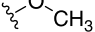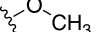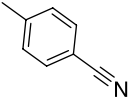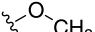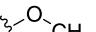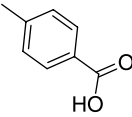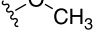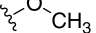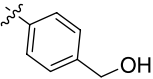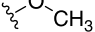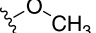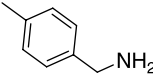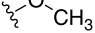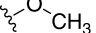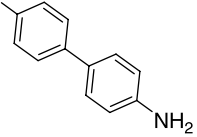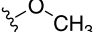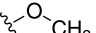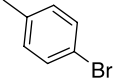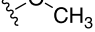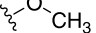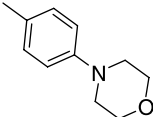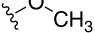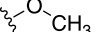
Compounds	R$_1$	R$_2$	R$_3$	R$_4$	IC$_{50}$ (nM)	p IC$_{50}$
CHK4308M50				H	74	7.13
CHK4308M51				H	48	7.32
CHK5944M2				H	2	8.70
CHK5944M3				H	25	7.60
CHK5944M4				H	7	8.15
CHK5944M5				H	2	8.70
CHK5944M6				H	25	7.60
CHK5944M7				H	779	6.11
CHK5944M8				H	355	6.45
CHK5944M10				H	73	7.14
CHK5944M13				H	6223	5.21

Table 1 – *continued*
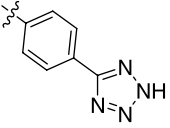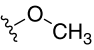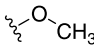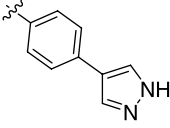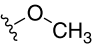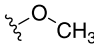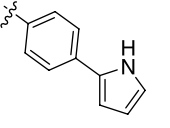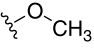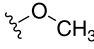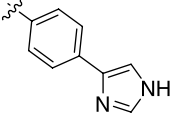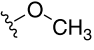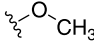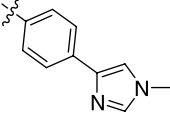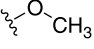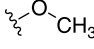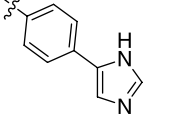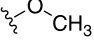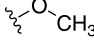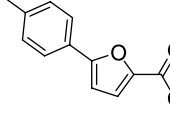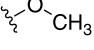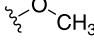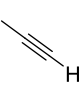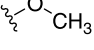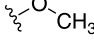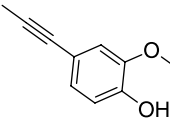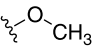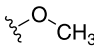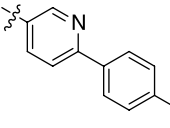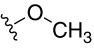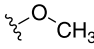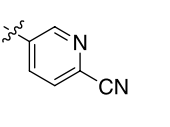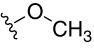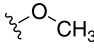
Compounds	R_1	R_2	R_3	R_4	IC_{50} (nM)	pIC_{50}
CHK5944M15				H	11	7.96
CHK5944M16				H	47	7.33
CHK5944M17				H	77	7.11
CHK5944M18				H	1260	5.90
CHK5944M19				H	1374	5.86
CHK5944M20				H	3709	5.43
CHK5944M21				H	3003	5.52
CHK5944M22				H	5140	5.29
CHK5944M24				H	5	8.30
CHK5944M28				H	0.5	9.30
CHK5944M29				H	0.8	9.10

Table 1 – *continued*
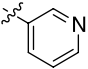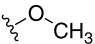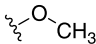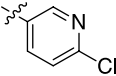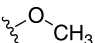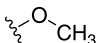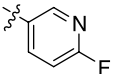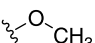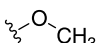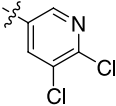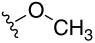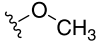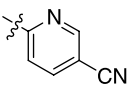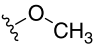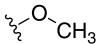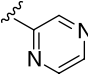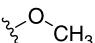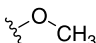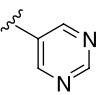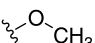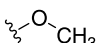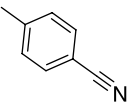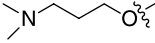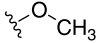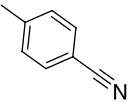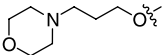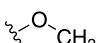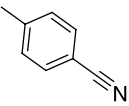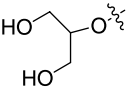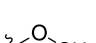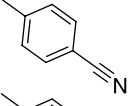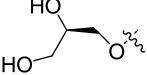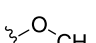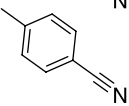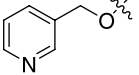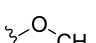
Compounds	R$_1$	R$_2$	R$_3$	R$_4$	IC$_{50}$ (nM)	p IC$_{50}$
CHK5944M30				H	15	7.82
CHK5944M31				H	4	8.40
CHK5944M32				H	2	8.70
CHK5944M35				H	16	7.80
CHK5944M37				H	44	7.36
CHK5944M38				H	89	7.05
CHK5944M39				H	44	7.36
CHK5944M40				H	4	8.40
CHK5944M41				H	3	8.52
CHK5944M42				H	3	8.52
CHK5944M43				H	6	8.22
CHK5944M44				H	14	7.85

Table 1 – *continued*
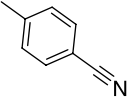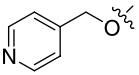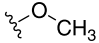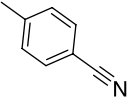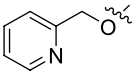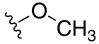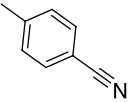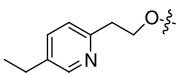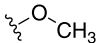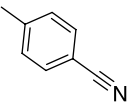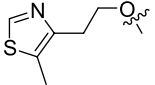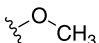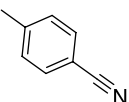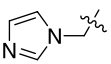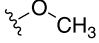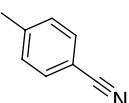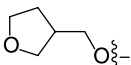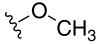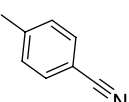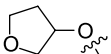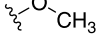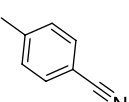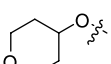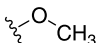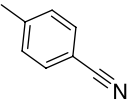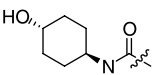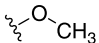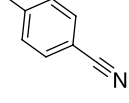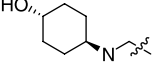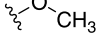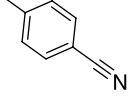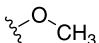
Compounds	R₁	R₂	R₃	R₄	IC₅₀ (nM)	pIC₅₀
CHK5944M45				H	20	7.70
CHK5944M46				H	10	8.00
CHK5944M47				H	77	7.11
CHK5944M48				H	9	8.05
CHK5944M49				H	2	8.70
CHK5944M50				H	3	8.52
CHK5944M51				H	2	8.70
CHK5944M52				H	1	9.00
CHK5944M53				H	3	8.52
CHK5944M54				H	17	7.77
CHK5944M55		OH		H	2	8.70

Table 2.   Actual and predicted inhibitory activities (pIC_{50}) and residuals of the training-set molecules, and docking ChemScores of CHK1 inhibitors.

No.	Compound numbers	ChemScore	pIC_{50}	Predicted	Residuals
1	CHK4308M10	43.39	9.000	8.822	0.178
2	CHK4308M11	43.56	8.398	8.961	−0.563
3	CHK4308M12	45.02	8.699	8.781	−0.082
4	CHK4308M13	45.24	8.222	8.323	−0.101
5	CHK4308M14	42.53	7.602	7.353	0.249
6	CHK4308M15	45.04	8.097	8.314	−0.217
7	CHK4308M16	45.82	8.097	8.098	−0.001
8	CHK4308M18	44.73	7.699	7.969	−0.270
9	CHK4308M19	43.50	8.301	8.425	−0.124
10	CHK4308M20	43.83	7.886	8.214	−0.328
11	CHK4308M21	43.31	7.523	7.385	0.138
12	CHK4308M22	44.77	7.638	7.691	−0.053
13	CHK4308M23	44.26	7.208	7.831	−0.623
14	CHK4308M24	43.63	8.301	8.154	0.147
15	CHK4308M27	43.21	10.000	9.689	0.311
16	CHK4308M28	45.98	9.097	9.006	0.091
17	CHK4308M29	42.83	9.699	9.316	0.383
18	CHK4308M31	44.35	9.155	8.839	0.316
19	CHK4308M32	45.62	9.000	9.034	−0.034
20	CHK4308M33	45.48	8.301	8.765	−0.464
21	CHK4308M36	42.49	9.222	9.066	0.156
22	CHK4308M37	44.29	8.699	8.778	−0.079
23	CHK4308M39	43.96	9.699	9.421	0.278
24	CHK4308M40	41.33	9.222	9.391	−0.169
25	CHK4308M42	39.12	8.699	8.522	0.177
26	CHK4308M44	42.31	8.522	8.773	−0.251
27	CHK4308M46	44.00	7.638	7.271	0.367
28	CHK4308M47	44.18	7.444	7.288	0.156
29	CHK4308M48	44.80	7.398	7.112	0.286
30	CHK4308M49	43.99	7.678	7.911	−0.233
31	CHK4308M5	43.12	8.699	8.781	−0.082
32	CHK4308M50	44.29	7.131	7.673	−0.542
33	CHK4308M7	43.86	9.155	8.893	0.262
34	CHK4308M8	46.22	8.699	8.717	−0.018
35	CHK4308M9	43.40	9.099	8.398	0.701
36	CHK2759M11	37.51	5.982	5.739	0.243
37	CHK2759M13	39.45	6.102	6.124	−0.022
38	CHK2759M14	38.91	6.015	5.662	0.353
39	CHK2759M15	40.31	5.796	6.002	−0.206
40	CHK2759M17	40.52	5.279	5.321	−0.042
41	CHK2759M18	40.42	6.220	6.127	0.093
42	CHK2759M19	35.72	6.907	6.491	0.416
43	CHK2759M20	37.69	7.658	7.601	0.057
44	CHK2759M21	39.25	7.699	7.454	0.245
45	CHK2759M22	35.38	7.823	7.91	−0.087
46	CHK2759M23	36.94	8.102	7.737	0.365
47	CHK2759M24	37.05	8.222	7.96	0.262
48	CHK2759M26	38.37	7.921	8.524	−0.603
49	CHK2759M28	36.08	7.161	7.541	−0.380
50	CHK2759M29	35.60	7.538	7.501	0.037
51	CHK2759M30	38.20	6.272	6.254	0.018
52	CHK2759M31	40.43	5.058	5.137	−0.079
53	CHK2759M32	40.03	5.317	5.384	−0.067
54	CHK2759M35	41.73	5.726	5.802	−0.076
55	CHK2759M36	39.07	5.189	4.842	0.347
56	CHK2759M37	41.12	8.699	8.531	0.168
57	CHK2759M40	47.68	8.131	8.081	0.050
58	CHK2759M41	48.52	8.208	8.099	0.109
59	CHK2759M42	44.21	8.398	8.548	−0.150
60	CHK2759M43	44.35	7.886	7.634	0.252

Table 2 – *continued*

No.	Compound numbers	ChemScore	$p\,IC_{50}$	Predicted	Residuals
61	CHK2759M44	40.62	8.444	8.421	0.023
62	CHK2759M7	38.46	6.338	6.925	− 0.587
63	CHK2759M8	37.26	6.089	6.192	− 0.103
64	CHK2759M9	37.74	5.832	5.977	− 0.145
65	CHK3618M11	46.11	8.921	8.981	− 0.060
66	CHK3618M12	45.50	8.678	8.711	− 0.033
67	CHK3618M13	46.36	9.131	9.167	− 0.036
68	CHK3618M16	46.18	6.680	7.246	− 0.566
69	CHK3618M19	44.35	8.357	8.412	− 0.055
70	CHK3618M21	41.66	7.921	7.436	0.485
71	CHK3618M22	43.65	7.824	7.633	0.191
72	CHK3618M24	39.99	8.301	8.615	− 0.314
73	CHK3618M25	41.79	8.638	8.593	0.045
74	CHK3618M33	43.40	9.619	9.066	0.553
75	CHK3618M34	42.42	8.638	8.702	− 0.064
76	CHK3618M35	44.99	9.081	8.908	0.173
77	CHK3618M37	43.87	9.259	9.063	0.196
78	CHK3618M38	45.76	9.367	8.817	0.550
79	CHK3618M39	40.95	9.292	9.599	− 0.307
80	CHK3618M40	46.44	9.678	9.022	0.656
81	CHK3618M41	47.03	9.252	9.141	0.111
82	CHK3618M5	43.65	5.862	6.021	− 0.159
83	CHK3618M6	42.84	7.620	7.936	− 0.316
84	CHK3618M7	44.76	8.032	8.165	− 0.133
85	CHK3618M9	44.00	8.113	7.905	0.208
86	CHK5944M10	36.01	7.137	6.899	0.238
87	CHK5944M13	39.24	5.206	5.190	0.016
88	CHK5944M15	40.73	7.959	8.139	− 0.180
89	CHK5944M16	42.84	7.328	7.233	0.095
90	CHK5944M17	40.42	7.114	6.802	0.312
91	CHK5944M19	37.50	5.862	6.385	− 0.523
92	CHK5944M2	43.02	8.699	8.902	− 0.203
93	CHK5944M20	38.68	5.431	5.164	0.267
94	CHK5944M21	39.59	5.522	5.651	− 0.129
95	CHK5944M22	38.12	5.289	5.579	− 0.290
96	CHK5944M24	34.22	8.301	8.125	0.176
97	CHK5944M28	40.54	9.301	9.472	− 0.171
98	CHK5944M30	32.86	7.824	7.752	0.072
99	CHK5944M31	34.64	8.398	8.003	0.395
100	CHK5944M32	32.69	8.699	8.351	0.348
101	CHK5944M35	35.13	7.796	7.870	− 0.074
102	CHK5944M37	32.86	7.357	7.629	− 0.272
103	CHK5944M38	32.11	7.051	7.285	− 0.234
104	CHK5944M39	29.26	7.357	7.315	0.042
105	CHK5944M4	34.32	8.155	7.742	0.413
106	CHK5944M40	34.03	8.398	8.615	− 0.217
107	CHK5944M42	36.51	8.523	8.816	− 0.293
108	CHK5944M43	38.50	8.222	8.383	− 0.161
109	CHK5944M44	36.64	7.854	7.367	0.487
110	CHK5944M45	35.62	7.699	7.773	− 0.074
111	CHK5944M47	36.19	7.114	7.302	− 0.188
112	CHK5944M48	36.37	8.046	8.445	− 0.399
113	CHK5944M49	35.47	8.699	8.705	− 0.006
114	CHK5944M5	34.87	8.699	8.571	0.128
115	CHK5944M51	34.65	8.699	8.417	0.282
116	CHK5944M53	35.03	8.523	8.421	0.102
117	CHK5944M54	36.83	7.770	7.947	− 0.177
118	CHK5944M55	36.39	8.699	8.624	0.075
119	CHK5944M6	37.32	7.602	7.279	0.323
120	CHK5944M7	35.30	6.108	6.811	− 0.703
121	CHK5944M8	34.26	6.450	6.235	0.215

Table 3. Actual and predicted inhibitory activities ($p\,IC_{50}$) and residuals of the test-set molecules, and docking ChemScores of CHK1 inhibitors.

No.	Compound numbers	ChemScore	$p\,IC_{50}$	Predicted	Residuals
1	CHK4308M17	46.45	7.745	8.265	−0.52
2	CHK4308M26	45.89	10.000	9.239	0.761
3	CHK4308M30	44.59	9.398	8.818	0.58
4	CHK4308M34	43.10	9.097	8.519	0.578
5	CHK4308M35	42.07	8.699	8.505	0.194
6	CHK4308M38	41.92	9.097	8.676	0.421
7	CHK4308M41	42.01	8.301	8.585	−0.284
8	CHK4308M43	45.35	8.000	8.387	−0.387
9	CHK4308M45	43.44	7.620	8.096	−0.476
10	CHK4308M51	45.01	7.319	7.569	−0.25
11	CHK4308M6	42.63	8.699	8.135	0.564
12	CHK2759M10	39.28	6.318	6.311	0.007
13	CHK2759M12	42.81	6.304	6.897	−0.593
14	CHK2759M16	36.23	5.690	6.265	−0.575
15	CHK2759M25	38.37	7.824	8.122	−0.298
16	CHK2759M27	39.12	7.921	7.697	0.224
17	CHK2759M38	45.28	8.180	8.542	−0.362
18	CHK3618M10	47.64	8.194	8.554	−0.36
19	CHK3618M15	44.39	8.108	8.225	−0.117
20	CHK3618M20	42.75	7.469	8.187	−0.718
21	CHK3618M23	42.42	8.149	8.348	−0.199
22	CHK3618M36	43.40	9.620	8.965	0.655
23	CHK3618M8	44.67	8.357	8.199	0.158
24	CHK5944M18	41.29	5.900	6.813	−0.913
25	CHK5944M29	32.61	9.097	8.496	0.601
26	CHK5944M3	33.18	7.602	7.637	−0.035
27	CHK5944M41	36.79	8.523	8.225	0.298
28	CHK5944M46	35.77	8.000	8.089	−0.089
29	CHK5944M50	36.97	8.523	7.794	0.729
30	CHK5944M52	34.22	9.000	8.116	0.884

pocket of CHK1 and used directly for CoMFA to explore the specific contributions of electrostatic and steric effects. Also, the conformations with the highest ChemScore for each ligand from the test set were selected. The $p\,IC_{50}$ values of the inhibitors are shown in Table 1 and the ChemScore for all the inhibitors is listed in Tables 2 and 3.

2.5 Comparative molecular field analysis

Steric and electrostatic interactions were calculated using the Tripos force field with a distance-dependent dielectric constant at all intersections in a regularly spaced (2 Å) grid taking an sp^3 carbon atom as steric probe and a $+1$ charge as electrostatic probe. The energy value cut-off was set to 30 kcal/mol. The partial least-squares (PLS) method was used to linearly correlate the CoMFA fields to the inhibitory activity values. The cross-validation analysis was performed using the leave-one-out (LOO) method, in which one compound is removed from the data set and its activity is predicted using the model derived from the rest of the dataset [26,31]. The optimum number of components at the lowest standard error of prediction was

applied to further analysis. Equal weights were assigned to steric and electrostatic fields using the CoMFA scaling option. To speed up the analysis and reduce noise, a minimum filter value of 2.0 kcal/mol was used for the standard deviation of field variables. Typically, the increase in q^2 with an additional component is less than 5%, and the model with the fewer components is recommended over the model with the slightly higher q^2 [32]. The optimum number of components is then used to derive the final QSAR model including all of the training-set compounds and to obtain the conventional correlation coefficient (r^2).

3. Results and discussion

3.1 Binding conformations docking study

Several evaluations about the accuracy of commonly used docking programs have concluded that many programs are able to reproduce the crystallographically determined binding modes, and GOLD is one of the most reliable docking programs [23–25]. In order to determine the probable binding conformations of these 1,4-dihydroin-deno[1,2-c]pyrazoles, GOLD was used to dock all
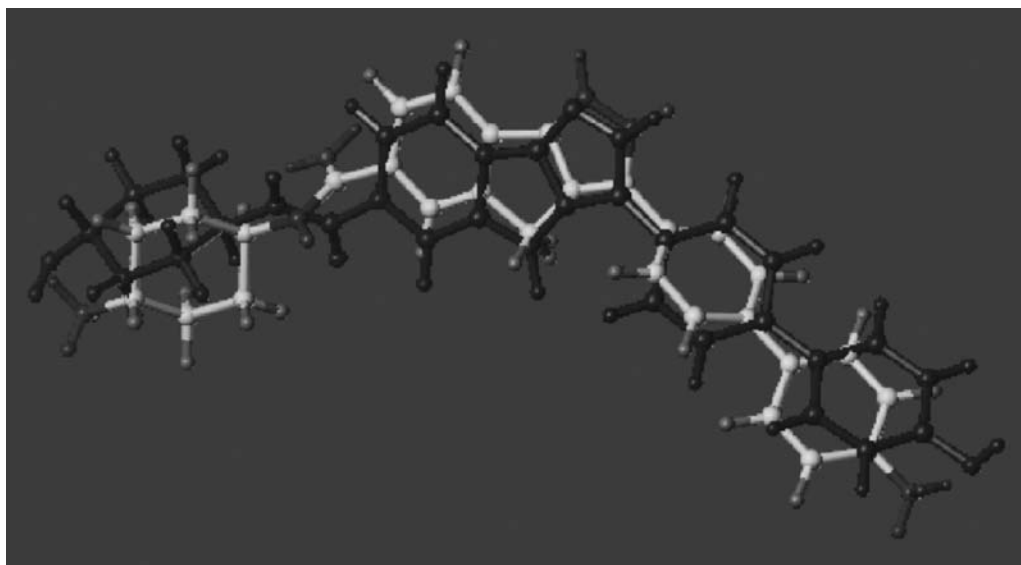
Figure 1. Binding conformations of the cocrystallised CHK2759M41 and redocked CHK2759M41 at the active sites of CHK1. (Black compound represents cocrystallised CHK2759M41 and white compound represents redocked CHK2759M41).

compounds into the active sites of CHK1. The docking reliability was validated using the known X-ray structure of CHK1 in complex with a small molecular ligand CHK2759M41. The root-mean-square deviation (RMSD) between the conformations of cocrystallised and redocked CHK2759M41 is 1.118 Å, suggesting that GOLD is able to generate the experimentally observed binding mode for CHK1 inhibitors and that the parameters set for the GOLD simulation is appropriate for reproduction of the X-ray structure. The superposition of docked structure and
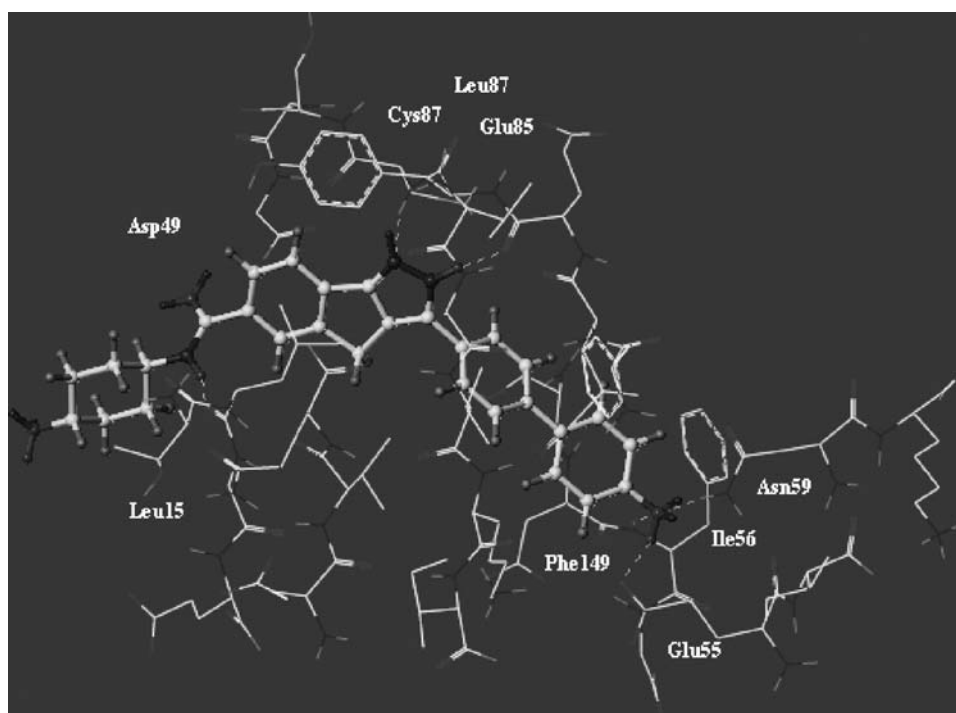
Figure 2. Position of docked inhibitor CHK2759M41 in the binding pocket of CHK1 H-bonds and interactions between CHK2759M41 and side chain residues.
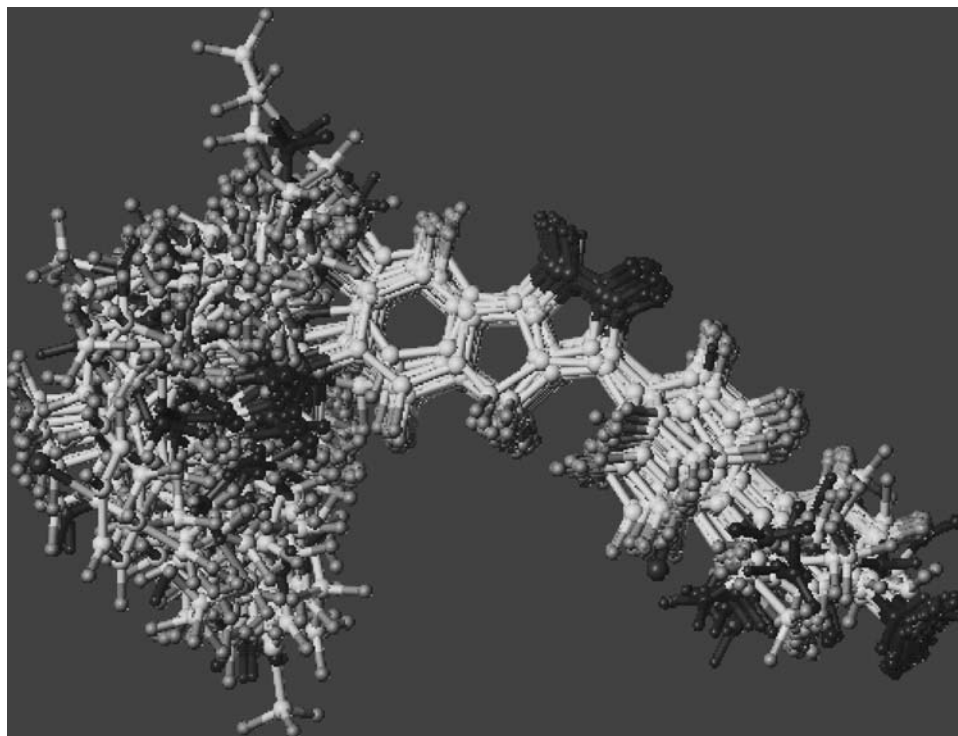
Figure 3.   Superimposition of 151 substituted 1,4-dihydroindeno[1,2-c]pyrazoles for 3D-QSAR studies.

crystal structure of CHK2759M41 is shown in Figure 1, which showed us that they take almost same binding position in the active sites of CHK1. According to the similar structure with the 1,4-dihydroindeno[1,2-c]pyrazoles shown in Table 1, the GOLD with the same parameters set for docking could be extended to search the binding conformations of the rest of the inhibitors against CHK1.

Figure 2 describes the interaction model of the docked inhibitor CHK2759M41 with CHK1. Inhibitor CHK2759M41 binds to the active site and makes several interactions with the hinge-binding region of the enzyme. As shown in Figure 2, the pyrazole of CHK2759M41 forms two hydrogen bonds with Glu85 and Cys87. Also, the hydroxyl group in the third position of CHK2759M41 forms its own hydrogen bonds to Glu55 and Asn59. The oxygen group in the sixth position of CHK2759M41 accepts an H-bond from the Cys379. The phenyl ring in CHK2759M41 interacts with the hydrophobic surface of the side chains of Leu84, Ile56, Val56 and Phe149. Also, the cyclohexane ring interacts with the hydrophobic surface of the side chains of Tyr86, Ser88, Thr14, Asp94 and Glu17. Figure 3 illustrates the probable binding conformational alignment for the 151 substituted 1,4-dihydroindeno[1,2-c]pyrazoles inhibitors chosen from the docked conformations.

3.2   CoMFA model

The structure–activity relationship of substituted 1,4-dihydroindeno[1,2-c]pyrazoles inhibitors of CHK1 was explored by CoMFA. PLS analysis was carried out for the 121 compounds in training set, and the result is listed in Table 4, which shows that a CoMFA model with a cross-validated q^2 of 0.534 for six components was built. The non-cross-validated PLS analysis with the six optimum components revealed a conventional r^2 value of 0.911, $F = 187.106$ and an estimated standard error of 0.352. The steric field descriptors explain 43.0% of the variance, while the electrostatic descriptors explain 57.0%. The predicted activities for all the 151 inhibitors versus their experimental activities with their residues are listed in

Table 4.   Summary of CoMFA analysis.

Parameters	CoMFA
Training set	–
PLS statistics	–
LOO	–
q^2 (CV correlation coefficient)	0.534
N (number of components)	6
Uncross-validated	–
r^2 (correlation coefficient)	0.911
SEE (SE of estimate)	0.352
F (F-ratio)	187.106
Field distribution	–
Steric	43.0%
Electrostatic	57.0%
Testing set	–
r^2 (correlation coefficient)	0.812
S (SE of prediction)	0.313
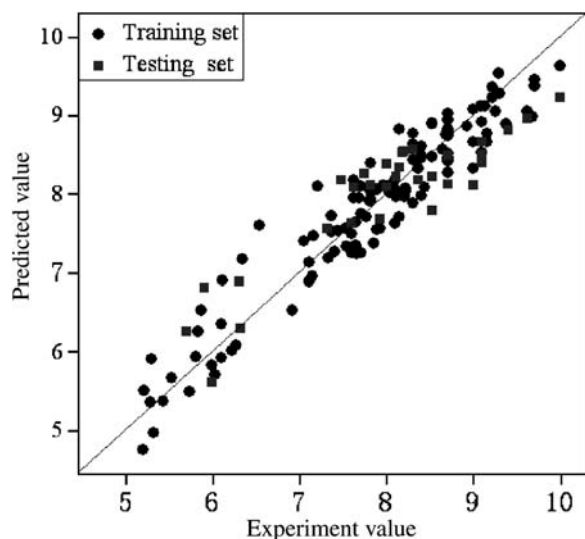
Figure 4.   Correlation between predicted activities by CoMFA model and the experimental pIC_{50} values of training set and testing set.

Tables 2 and 3, and the correlation between the predicted activities and the experimental activities is depicted in Figure 4. Tables 2–4 demonstrate that the activities predicted by the constructed CoMFA model are in good agreement with the experimental data, suggesting that a reliable CoMFA model was successfully constructed.

To visualise the information content of the derived 3D-QSAR models, CoMFA contour maps were generated. The CoMFA contour maps of steric and electrostatic fields are shown in Figures 5 and 6. In the CoMFA steric field, the green contours (contribution level of 80%) represent an additional steric group that confers an increased activity, while yellow contours (contribution level of 20%)

represent a bulky group that results in a decreased activity. Similarly, the blue contours indicate regions where the addition of electropositive substituent increases activity (contribution level of 80%); red indicates regions where the addition of an electronegative substituent increases activity (contribution level of 20%).

The CoMFA steric contours of the molecule CHK2759M41 are displayed in Figure 5. A large green region (G1) near the sixth-position of CHK2759M41 indicates that a bulky substituent is preferred in that position to produce higher inhibitory activity. This is in agreement with the fact that the inhibitory activities of compounds CHK2759M38 and CHK2759M42 with more bulky substituent (with aliphatic hydrocarbon) in G1 are higher than compound CHK3618M5 (with only an H atom in that position). Additionally, the highly active compounds CHK2759M39 and CHK2759M41 both have a larger substituent, the cyclohexyl substituent, in this area. Compounds from CHK4308M5 to CHK4308M13, which possess an aliphatic amine at the terminus of G1 position, show an activity with IC_{50} of nanomolar values against CHK1. Compounds with hetero-aromatic substituent on the sixth position (CHK4308M16 to CHK4308M24 and CHK2759M44 to CHK2759M49) also show good activity against CHK1, although they are less potent than the analogues with aliphatic amines group. Compounds CHK4308M26 and CHK4308M27 with diol group in that position are the most potent CHK1 inhibitors identified in this series with picomolar IC_{50} values. Compounds with cyclic substituent in the sixth position (CHK4308M28 to CHK4308M31 and CHK5944M50 to CHK5944M52) of those inhibitors exhibit sub-nanomolar potencies against CHK1. So this large volume (G1) predicted by the CoMFA model is in agreement with the structures of inhibitors and receptor.
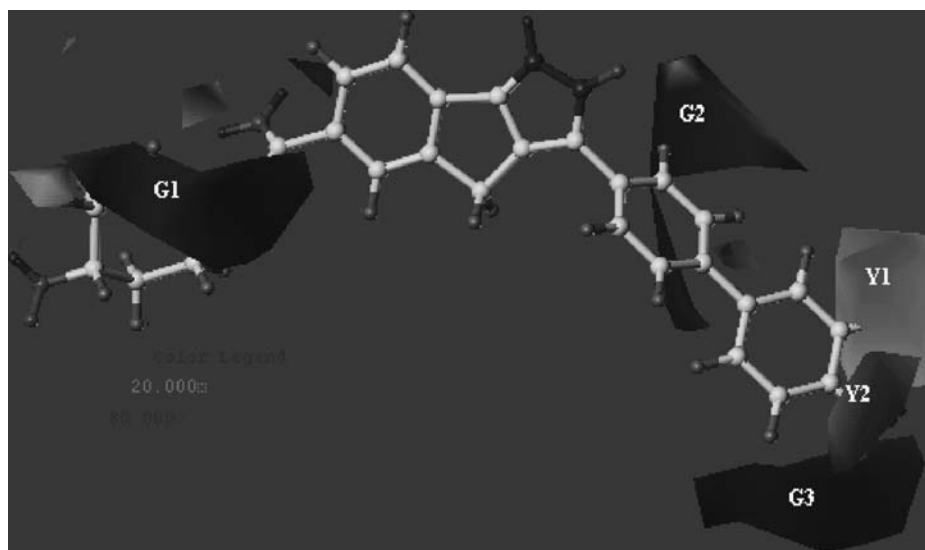
Figure 5.   CoMFA steric field distribution contour map in combination with inhibitor CHK2759M41.
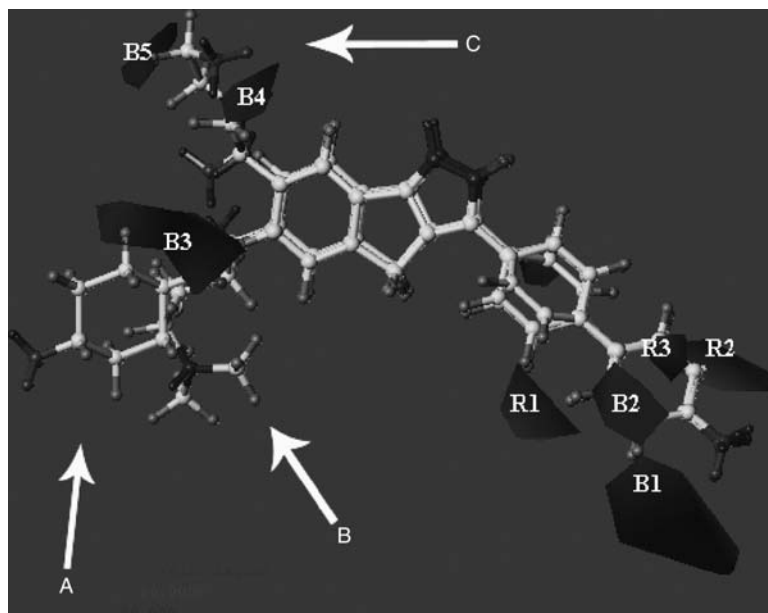
Figure 6.   CoMFA electrostatic field distribution contour map in combination with inhibitors CHK2759M41 (A), CHK4308M7 (B) and CHK3618M24 (C).

G2 is next to the third position of the 1,4-dihydroindeno[1,2-c]pyrazoles, which indicates that steric bulk is favoured for activity in this area. For example, the activities of compounds from CHK5944M40 to CHK5944M55 with benzene ring were shown to be more active than compound CHK5944M22 with acetylene group.

A large region of green contour (G3) near the third position of the CHK2759M41 suggests that a bulky group would increase the activity. For example, the activities of compounds from CHK2759M37 to CHK2759M42 (with hydroxybenzenes group) are higher than compounds from CHK2759M22 to CHK2759M29 (with carboxy group). Region (G3) is also in agreement with the receptor structure. The nearest residues are Leu84, Ile56, Val56 and Phe149, which all have hydrophobic side chains. R3 substituent with hydroxybenzene groups has hydrophobic interaction with the side chains of Leu84, Ile56, Val56 and Phe149.

Two yellow contours (Y1 and Y2) were observed, which suggest that compounds with substituents in this area are less active than those without substituents in this position. Figure 2 shows that residues Phe149, Glu55, Lys38 and Leu84 in the binding pocket of the CHK1 are in the distance of less than 3.0 Å to Y1 and Y2. Therefore, any larger substitutes may lead to steric collision with those residues mentioned below. One finding further supports this opinion that the activity of compound CHK2759M41 decreases quickly when the —OH groups are replaced by bulky groups, just like CHK2759M31, which has a benzene ring group in Y1 and Y2.

The electrostatic contour map of the CoMFA model is shown in Figure 6. To facilitate the visualisation, the compounds CHK2759M41 (A), CHK4308M7 (B) and CHK3618M24 (C) are superposed on the map.

A red contour (R1) indicates that the electronegative group at this position is essential for activity. For example, the high active compounds CHK2758M22, CHK2758M23, CHK2758M24, CHK2758M25, CHK2758M26, CHK2758M27 and CHK2758M28 have electronegative groups (with carboxy group) located in this red contour. Also, docking studies show that compounds with a carboxy group can form H-bonds with the positively charged amino group of Lys38. The red region explains why the R3 substituents containing hetero-aromatic group just like CHK5944M29 to CHK5944M32 with electronegative groups show less than 15 nM IC_{50} values against CHK1.

Two red contours (R2 and R3), which are observed next to the benzene ring, are contributed by the compounds from CHK5944M40 to CHK5944M50 with nitrile group. Nitrile groups have an overall negative-charge and hence show reasonable activity. Furthermore, Asn59 containing positive groups rather near this region (R2 and R3) has a strong electrostatic interaction with the negatively charged substituent groups of those inhibitors. The docking study also shows that the —NH groups in Asn59 forms H-bonds with the —OH groups of compounds from CHK4308M5 to CHK4308M52 on that position.

Two large blue (B1 and B2) regions near Glu55, Gly150 and Asp148 suggest that electropositive substituent in this part would increase the inhibitory activity. Most of those inhibitors with benzene ring in that position interact with the Phe83 and form a Π–Π conjugate. So, chemicals with two benzene rings as substituents in the

third position produce good activity against CHK1 than the compounds with one benzene ring.

A large blue contour (B3) is noticed in the sixth-position of CHK2759M41 (A). As shown in Figure 6, a small area of blue (B4) contour around the seventh position of CHK4308M7 (B) indicates that an electropositive substituent is favoured for activity in this area. As the experimental data show, compounds CHK4308M7, CHK4308M9, CHK4308M26, CHK4308M27 and CHK4308M28, which have a —OMe group on that position, have good pIC$_{50}$ values from 0.1 to 1 nM. Also, the seventh position with —OMe group can bind to the enzyme by making van der Waals contact within a small hydrophobic pocket formed by the side chain of Tyr86 and the methylene of Gly90. In Figure 6, the blue contour region (B5) shows that electropositive groups are favourable in this region. Inhibitors CHK4308M42 and CHK3618M24(C) which contain partially positive charged groups (—NH$_2$) in this region show higher pIC$_{50}$ values.

3.3 Validation of the 3D-QSAR models

The 30 randomly selected compounds (Table 3) were used as the testing set to verify the constructed CoMFA model. The calculated results are listed in Table 3 and displayed in Figure 4. The predicted pIC$_{50}$ values are in good agreement with the experimental data, and the correlation coefficient (r^2) is 0.812 with a statistically tolerable error. The test results indicate that the CoMFA model would be reliably used in new the inhibitor design.

4. Conclusions

In this study, a highly predictive CoMFA model was developed on a series of 1,4-dihydroindeno[1,2-c]pyrazoles derivatives of CHK1 inhibitors based on the alignment conformations generated from the docking study. The satisfactory model was constructed with LOO cross-validation q^2 and conventional r^2 values of 0.534 and 0.911, respectively. The binding conformations of all 1,4-dihydroindeno[1,2-c]pyrazoles derivatives were predicted by molecular docking. The reliability of the model was further verified using the compounds in the test set. Higher degree of electronegativity of the substituent R1 (e.g. carboxy group) is favourable to the activity of the compound, because there is a red area (R1) in 3D electrostatic contour map towards it. Moreover, the 3D-QSAR results suggest that 1,4-dihydroindeno[1,2-c]pyrazoles can form two hydrogen bonds with Cys87 and Glu85 in the third position. So, hydroxybenzene is favourable in the third position. In addition, a large substituent in the sixth position of 1,4-dihydroindeno[1,2-c]pyrazoles can increase the activity of these compounds, because these compounds can effectively form hydrophobic interactions with Tyr86, Ser88, Thr14, Asp94 and Glu17. Electropositive substituent groups with —OMe in the seventh position of these inhibitors are favourable to the bioactivity. These results demonstrate the power of a combined docking and 3D-QSAR approach to explore the probable binding conformations of compounds at the active site of the protein target, and further provide useful information in understanding the structural and chemical features of 1,4-dihydroindeno[1,2-c]pyrazoles derivatives in designing and finding new potential inhibitors against CHK1.

Note

1. Email: zlzuo@sp.edu.sg

References

[1] L.H. Hurley, *DNA and its associated processes as targets for cancer therapy*, Nat. Rev. Cancer 2 (2002), pp. 188–200.
[2] Z.F. Tao, G.Q. Li, Y.S. Tong, K.D. Stewart, Z. Chen, M.H. Bui, P. Merta, C. Park, P. Kovar, H.Y. Zhang, H.L. Sham, S.H. Rosenberg, T.J. Sowin, and N.H. Lin, *Discovery of 4′-(1,4-dihydro-indeno[1,2-c]pyrazol-3-yl)-benzonitriles and 4′-(1,4-dihydro-indeno[1,2-c]pyrazol-3-yl)-pyridine-2′-carbonitriles as potent checkpoint kinase 1 (Chk1) inhibitors*, Bioorg. Med. Chem. Lett. 17 (2007), pp. 5944–5951.
[3] A. Sancar, L.A. Lindsey-Boltz, K. Unsal-Kacmaz, and S. Linn, *Molecular mechanisms of mammalian DNA repair and the DNA damage checkpoints*, Annu. Rev. Biochem. 73 (2004), pp. 39–85.
[4] B.B. Zhou and J. Bartek, *Targeting the checkpoint kinases: chemosensitization versus chemoprotection*, Nat. Rev. Cancer 4 (2004), pp. 216–225.
[5] M.B. Kastan and J. Bartek, *Cell-cycle checkpoints and cancer*, Nature 432 (2004), pp. 316–323.
[6] Z.F. Tao, L. Wang, K.D. Stewart, Z. Chen, W. Gu, M. Bui, P. Merta, H. Zhang, P. Kovar, E. Johnson, C. Park, R. Judge, S. Rosenberg, T. Sowin, and N.H. Lin, *Structure-based design, synthesis, and biological evaluation of potent and selective macrocyclic checkpoint kinase 1 inhibitors*, J. Med. Chem. 50 (2007), pp. 1514–1527.
[7] N. Walworth, S. Davey, and D. Beach, *Fission yeast Chk1 protein kinase links the rad checkpoint pathway to cdc2*, Nature 363 (1993), pp. 368–371.
[8] Y. Chen and Y. Sanchez, *Chk1 in the DNA damage response: conserved roles from yeasts to mammals*, DNA Repair 3 (2004), pp. 1025–1032.
[9] Q. Liu, S. Guntuku, X.S. Cui, S. Matsuoka, D. Cortez, K. Tamain, G.B. Luo, S.C. Rivera, F. Demya, A. Bradley, L.A. Donehower, and S.J. Elledge, *Chk1 is an essential kinase that is regulated by Atr and required for the G2/M DNA damage checkpoint*, Genes Dev. 14 (2000), pp. 1448–1459.
[10] R.T. Abraham, *Cell cycle checkpoint signaling through the ATM and ATR kinases*, Genes Dev. 15 (2001), pp. 2177–2196.
[11] Y. Tong, A. Claiborne, M. Pyzytulinska, Z.F. Tao, K.D. Stewart, P. Park, P. Kovar, Z. Chen, R.B. Credo, R. Guan, P.L. Merta, H. Zhang, J. Bouska, E.A. Everitt, B.P. Murry, D. Hickman, T.J. Stratton, J. Wu, S.H. Rosenberg, H.L. Sham, T.J. Sowin, and N.H. Lin, *1,4-Dihydroindeno[1,2-c]pyrazoles as potent checkpoint kinase 1 inhibitors: Extended exploration on phenyl ring substitutions and preliminary ADME/PK studies*, Bioorg. Med. Chem. Lett. 17 (2007), pp. 3618–3623.
[12] P.R. Graves, L. Yu, J.K. Schwarz, J. Gales, E.A. Sausville, P.M. O'Connor, and H. Piwnica-Worms, *The chk1 protein kinase and the Cdc25C regulatory pathways are targets of the anticancer agent UCN-01*, J. Biol. Chem. 275 (2000), pp. 5600–5605.

[13] X. Jiang, B. Zhao, R. Britton, L.Y. Lim, D. Leong, J.S. Sanghera, B.B.S. Zhou, S. Piers, R.J. Andersen, and M. Roberge, *Inhibition of Chk1 by the G2 DNA damage checkpoint inhibitor isogranulatimide*, Mol. Cancer Ther. 3 (2004), pp. 1221–1227.

[14] D. Curman, B. Cinel, D.E. Williams, N. Rundle, W.D. Block, A.A. Goodarzi, J.R. Hutchins, P.R. Clarke, B.B.S. Zhou, S.P. Lees-Miller, R.J. Andersen, and M. Roberge, *Inhibition of the G2 DNA damage checkpoint and of protein kinases Chk1 and Chk2 by the marine sponge alkaloid debromohymenialdisine*, J. Biol. Chem. 276 (2001), p. 17914.

[15] P.D. Lyne, P.W. Kenny, D.A. Cosgrove, C. Deng, S. Zabludoff, S. Ashwell, and J.J. Wendoloski, *Identification of compounds with nanomolar binding affinity for checkpoint kinase-1 using knowledge-based virtual screening*, J. Med. Chem. 47 (2004), pp. 1962–1968.

[16] N. Foloppe, L.M. Fisher, R. Howes, P. Kierstan, A. Potter, A.G.S. Robertson, and A.E. Surgenor, *Structure-based design of novel Chk1 inhibitors: Insights into hydrogen bonding and protein–ligand affinity*, J. Med. Chem. 48 (2005), pp. 4332–4345.

[17] M.E. Fraley, J.T. Steen, E.J. Brnardic, K.L. Arrington, K.L. Spencer, B.A. Hanney, Y. Kim, G.D. Hartman, S.M. Stirdivant, B.A. Drakas, K. Rickert, E.S. Walsh, K. Hamilton, C.A. Buser, J. Hardwick, W. Tao, S.C. Beck, X. Mao, R.B. Lobell, L. Sepp-Lorenzino, Y. Yan, M. Ikuta, S.K. Munshi, L.C. Kuo, and C. Kreatsoulas, *3-(Indol-2-yl)indazoles as Chek1 kinase inhibitors: Optimization of potency and selectivity via substitution at C6*, Bioorg. Med. Chem. Lett. 16 (2006), pp. 6049–6053.

[18] Z.J. Ni, P. Barsanti, N. Brammeier, A. Diebes, D.J. Poon, S. Ng, S. Pecchi, K. Pfister, P.A. Renhowe, S. Ramurthy, A.S. Wagman, D.E. Bussiere, V. Le, Y. Zhou, J.M. Jansen, S. Ma, and T.G. Gesner, *4-(Aminoalkylamino)-3-benzimidazole-quinolinones as potent CHK-1 inhibitors*, Bioorg. Med. Chem. Lett. 16 (2006), pp. 3121–3124.

[19] Y. Tong, A. Claiborne, K.D. Stewart, P. Park, P. Kovar, Z. Chen, R.B. Credo, W.Z. Gu, S.L. Gwaltney, R.A. Judge, H. Zhang, S.H. Rosenberg, H.L. Sham, T.J. Sowin, and N.H. Lin, *Discovery of 1,4-dihydroindeno[1,2-c]pyrazoles as a novel class of potent and selective checkpoint kinase 1 inhibitors*, Bioorg. Med. Chem. Lett 15 (2007), pp. 2759–2767.

[20] Z.F. Tao, G. Li, Y. Tong, Z. Chen, P. Merta, H. Zhang, P. Kovar, S. Rosenberg, H.L. Sham, T.J. Sowin, and N.H. Lin, *Synthesis and biological evaluation of 4′-(6,7-disubstituted-2,4-dihydro-indenol]1,2-c]pyrazol-3-yl)-biphenyl-4-ol as potent Chk1 inhibitors*, Bioorg. Med. Chem. Lett. 15 (2007), pp. 4308–4315.

[21] M.D.M. AbdulHameed, A. Hamza, J. Liu, and C.G. Zhan, *Combined 3D-QSAR modeling and molecular docking study on indolinone derivatives as inhibitors of 3-phosphoinositide-dependent protein kinase-1*, J. Chem. Inf. Model. 48 (2008), pp. 1760–1772.

[22] G. Jones, P. Willett, R.C. Glen, A.R. Leach, and R. Taylor, *Development and validation of a genetic algorithm for flexible docking*, J. Mol. Biol. 267 (1997), pp. 727–748.

[23] X. Ma, L. Zhou, Z.L. Zuo, J. Liu, M. Yang, and R.W. Wang, *Molecular docking and 3D QSAR studies of substituted 2,2-bisaryl-bicycloheptanes as human 5-lipoxygenase-activating protein (FLAP) inhibitors*, QSAR Comb. Sci. 27 (2008), pp. 1083–1091.

[24] M.D. Eldridge, C.W. Murray, T.R. Auton, G.V. Paolini, and R.P. Mee, *Empirical scoring functions: I. The development of a fast empirical scoring function to estimate the binding affinity of ligands in receptor complexes*, J. Comput.-Aided Mol. Des. 11 (1997), pp. 425–445.

[25] C.A. Baxter, C.W. Murray, D.E. Clark, D.R. Westhead, and M.D. Eldridge, *Flexible docking using tabu search and an empirical estimate of binding affinity*, Proteins 33 (1998), pp. 367–382.

[26] M.L. Verdonk, J.C. Cole, M.J. Hartshorn, C.W. Murray, and R.D. Taylor, *Improved protein-ligand docking using GOLD*, Proteins 52 (2003), pp. 609–623.

[27] P. Yi, X. Fang, and M. Qiu, *3D-QSAR studies of checkpoint kinase weel inhibitors based on molecular docking, CoMFA and CoMSIA*, Eur. J. Med. Chem. 43 (2008), pp. 925–938.

[28] P. Yi and M. Qiu, *3D-QSAR and docking studies of aminopyridine carboxamide inhibitors of c-Jun N-terminal kinase-1*, Eur. J. Med. Chem. 43 (2008), pp. 604–613.

[29] S.J. Teague, *Implications of protein flexibility for drug discovery*, Nat. Rev. Drug Discov. 2 (2003), pp. 527–541.

[30] K. Gunasekaran and R. Nussinov, *How different are structurally flexible and rigid binding sites? Sequence and structural features discriminating proteins that do and do not undergo conformational change upon ligand binding*, J. Mol. Biol. 365 (2007), pp. 257–273.

[31] T.A. Halgren, *Maximally diagonal force constants in dependent angle-bending coordinates. II. Implications for the design of empirical force fields*, Am. J. Chem. Soc. 112 (1990), pp. 4710–4723.

[32] B.L. Podlogar and D.M. Ferguson, *QSAR and CoMFA: a perspective on the practical application to drug discovery*, Drug Des. Discov. 17 (2000), pp. 4–12.